ROYAL SOCIETY OF CHEMISTRY

PAPER

Check for updates

Color tuning of multi-resonant thermally activated delayed fluorescence emitters based on fully fused polycyclic amine/carbonyl frameworks†‡

John Marques dos Santos, [iD] [a] Chin-Yiu Chan, [iD] [c] Shi Tang, [iD] [d] David Hall, [iD] [ab] Tomas Matulaitis, [iD] [a] David B. Cordes, [iD] [a] Alexandra M. Z. Slawin, [iD] [a] Youichi Tsuchiya, [iD] [c] Ludvig Edman, [iD] *[d] Chihaya Adachi, [iD] *[c] Yoann Olivier [iD] *[b] and Eli Zysman-Colman [iD] *[a]

Two novel π-extended amine/carbonyl-based multi-resonance thermally activated delayed fluorescence (MR-TADF) emitters have been designed and synthesized. The two emitters are isomeric, composed of nine fused rings and show green-yellow emission. **Sym-DiDiKTa** and **Asym-DiDiKTa** possess *tert*-butyl groups distributed in a symmetrical and asymmetrical fashion, respectively, which significantly impact the single-crystal packing structure. The two compounds possess similar singlet–triplet energy gaps, ΔE_{ST}, of around 0.23 eV, narrowband emission characterized by a full-width at half-maximum, FWHM, of 29 nm and a photoluminescence quantum yield, Φ_{PL}, of 70% and 53% for the symmetric and asymmetric counterparts, respectively, in toluene. Investigation in OLEDs demonstrated that the devices with **Sym-DiDiKTa** and **Asym-DiDiKTa** displayed electroluminescence maxima of 543 and 544 nm, and maximum external quantum efficiencies (EQE$_{max}$) of 9.8% and 10.5%, respectively. The maximum EQE was further improved to 19.9% by employing a hyperfluorescence strategy. We further present the first example of a neutral MR-TADF emitter incorporated in a LEC device where **Sym-DiDiKTa** acts as the emitter. The LEC shows a λ_{EL} at 551 nm and FWHM of 60 nm with luminance of 300 cd m^{-2} and a fast turn-on time of less than 2 s to 100 cd m^{-2}.

10th Anniversay statement

The journal of Materials Chemistry C has been one of our favourite journals for electroluminescent materials and device research. The quality and breadth of the science covered in the journal particularly in the area of emitter development for electroluminescent devices has been excellent. It is always a pleasure to peruse each week's table of contents and to then read exciting and new science in optoelectronic materials. We look forward to the next 10 years and beyond and will continue to support JMCC.

[a] *Organic Semiconductor Centre, EaStCHEM School of Chemistry, University of St Andrews, St Andrews, KY16 9ST, UK. E-mail: eli.zysman-colman@st-andrews.ac.uk*

[b] *Laboratory for Computational Modeling of Functional Materials, Namur Institute of Structured Matter, University of Namur, Rue de Bruxelles, 61, 5000 Namur, Belgium. E-mail: yoann.olivier@unamur.be*

[c] *Center for Organic Photonics and Electronics Research (OPERA), Kyushu University, Motooka 744, Nishi-ku, Fukuoka 819-0395, Japan. E-mail: adachi@cstf.kyushu-u.ac.jp*

[d] *The Organic Photonics and Electronics Group, Department of Physics, Umea University, SE-90187 Umea, Sweden. E-mail: ludvig.edman@umu.se*

† The research data supporting this publication can be accessed at https://doi.org/10.17630/f844ce22-cf6b-413d-ae79-70e2e38a1f74

‡ Electronic supplementary information (ESI) available: A summary of prior examples of carbonyl-containing MR-TADF emitters, experimental details, synthesis procedures and characterization data, NMR spectra, HRMS, HPLC, X-ray crystallographic data, supplemental photophysical data, electrochemical data, *xyz* coordinate file for computations. CCDC 2225501–2225503. For ESI and crystallographic data in CIF or other electronic format see DOI: https://doi.org/10.1039/d3tc00641g

Introduction

Organic light-emitting diodes (OLEDs) have now matured as a technology and are now integrated in efficient, flexible and ultra-high contrast next-generation displays.[1,2] Organic thermally activated delayed fluorescence (TADF) materials are increasingly viewed as an attractive alternative emitter class to phosphorescent complexes that contain noble metals as they do not contain scarce elements yet can likewise harvest both singlet and triplet excitons in the device to generate light at comparable efficiencies.[3–7] Unlike phosphorescent OLEDs that funnel the emitting excitons *via* the lowest-lying triplet excited state, TADF compounds convert triplet excitons into singlets *via* reverse intersystem crossing (RISC),[8,9] which is possible at ambient temperatures due to the small S_1–T_1 energy gap, ΔE_{ST}.[10] Compounds that possess a small

This journal is © The Royal Society of Chemistry 2023

J. Mater. Chem. C, 2023, 11, 8263–8273 | 8263

ΔE_{ST} show a small overlap of the electron density between the highest occupied molecular orbital (HOMO) and lowest unoccupied molecular orbital (LUMO). To adhere to this requirement, the great majority of organic TADF emitters are based on a highly twisted donor-acceptor architecture and emit from a long-range charge transfer (LRCT) state.[7] This strategy, however, leads to molecules for which the conformational space is large in the excited state[11,12] that manifests in broadband emission with full width half maximum (FWHM) values of around 70–100 nm.[13] This is unattractive to the display industry as the color purity of these devices is poor and color filters must therefore be used to meet the industry standards for red, green and blue pixels. Hence, significant effort has been devoted in recent years to suppress vibrational and conformational relaxation within the emitter through the development of narrowband emitters.[14–20]

An exciting molecular design strategy to achieve these requirements was introduced by Hatakeyama and co-workers and relies typically on p- and n-doped nanographenes.[21,22] Termed multiple resonance (or multiresonant) TADF (MR-TADF) emitters, these compounds possess small-to-moderate ΔE_{ST} values, narrowband emission (with FWHM typically < 30 nm) and limited positive solvatochromism due to the short-range charge transfer (SRCT) nature of the emissive S_1.[22] Maximum external quantum efficiencies (EQE$_{max}$) as high as 34% for deep blue,[22] 40% for sky-blue,[23] 35%[24] for green and 36% for red[25] have been achieved for OLEDs containing MR-TADF emitters comprised of boron–nitrogen (B/N) doped polycyclic aromatic frameworks. Recently, the library of MR-TADF emitters has been expanded to contain boron–oxygen (B/O)-based emitters[26] and carbonyl–nitrogen (C=O/N)-based emitters[14–19] as well as C=O/N/O-,[17,27,28] C=O/N/S-[17,29] and C=O/N/SO$_2$-based[29] emitters.

While the recent conceptual progress in MR-TADF emitter design has delivered a burgeoning number of efficient B/N-doped compounds that emit across the entirety of the visible spectrum,[30,31] few tactics have been advanced to exploit the promising class of C=O/N-based MR-TADF emitters, which are represented by the emitter **DiKTa** (Fig. 1).[14–19,32,33] Recently,

Yasuda *et al.* reported a linearly extended C=O/N-based emitter, **QA-2** (Fig. 1) displaying TADF in 3 wt% PPCz doped film, with a ΔE_{ST} of 0.19 eV.[27] Similar to the design strategy used for *ν*-DABNA, where the central ring is functionalized with *meta*-disposed B–π–B and N–π–N groups, **QA-2** also contains *meta*-disposed C=O–π–C=O and N–π–N, which leads to an improvement of the TADF properties over the parent compound **DiKTa**, with a faster delayed lifetime (48 μs in 3 wt% PPCz and 93.3 μs in 5 wt% mCP, respectively). Despite the apparent increased conjugation length, a slightly blue-shifted λ_{PL} of 465 nm in toluene was observed for **QA-2**, compared to that of **DiKTa** (ΔE_{ST} of 0.15 eV and λ_{PL} of 473 nm in toluene).[15] The OLED with **QA-2** showed an EQE$_{max}$ of 19.0%. Our group has recently reported a helically chiral isomer of **QA-2** that contains *meta*-disposed C=O–π–C=O and N–π–N skeleton. Enantiomers of **Hel-DiDiKTa** (Fig. 1)[34] display circularly polarized luminescence (CPL), with a $|g_{PL}|$ of 4×10^{-4}, but likewise, its λ_{PL} (473 nm) is similar to that of **DiKTa**.

The exploitation of *para*-disposed functional groups to generate π-extended skeletons is a powerful strategy to tune the photophysical properties of MR-TADF emitters to the red.[25,35] Yasuda and co-workers have adopted this strategy where both the B–π–B and N–π–N-based groups are *para*-linked to construct red MR-TADF emitters such as **BBCz-R** (Fig. 1) that exhibits a λ_{PL} of 615 nm and a narrow FWHM of 21 nm (0.07 eV) in dilute toluene solution.[31] This strategy has also been used to generate B/O and B/S derivatives as shown in Fig. 1.[36,37] Remarkably, among the many MR-TADF emitters reported, comprehensive studies on compounds containing *para*-C=O–π–C=O and N–π–N frameworks have not as of yet been presented. In this context, expanding the chemical space explored in ketone-based MR-TADF emitters is desired.

Herein, we present two new isomeric π-extended C=O/N-based polycyclic aromatic compounds based on the annellation of two triangulene **DiKTa** units to form tetraketone structures. Differently from **QA-2** and **Hel-DiDiKTa**, the central ring in each of **Sym-DiDiKTa** and **Asym-DiDiKTa** is functionalized with *para*-C=O–π–C=O and N–π–N groups, these molecules represent
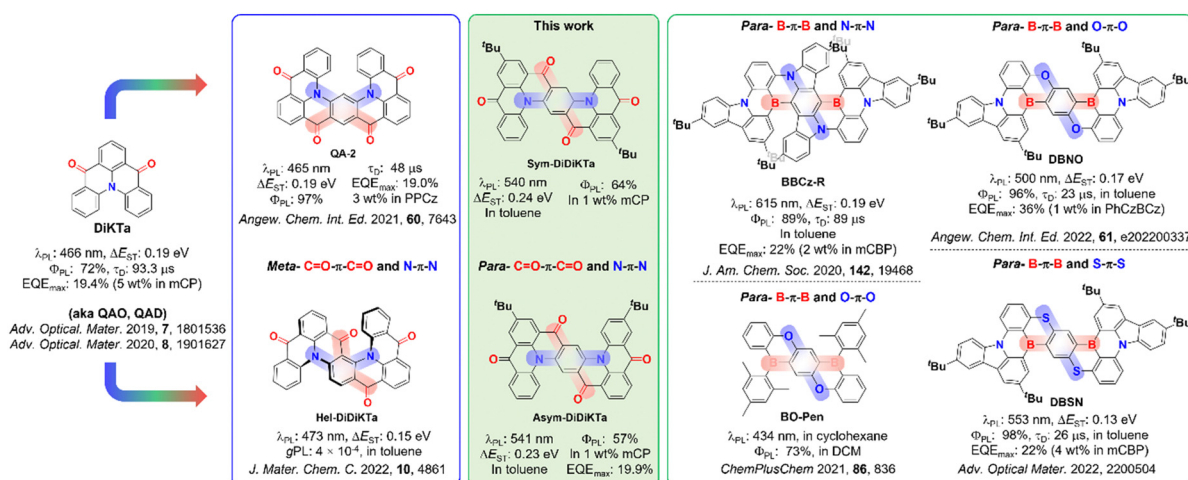

Fig. 1 Schematical representation of the molecular design discussed in this work.[15,27,31,34,36,37,42]

8264 | *J. Mater. Chem. C*, 2023, **11**, 8263–8273

This journal is © The Royal Society of Chemistry 2023

the first ketone-based MR-TADF examples of their kind (Fig. 1).[17–19,33] **Sym-DiDiKTa** is composed of nine fully fused rings with symmetrically arranged *tert*-butyl substituents while the *tert*-butyl groups are disposed asymmetrically in **Asym-DiDiKTa**. Both emitters show moderate ΔE_{ST} of around 0.23 eV, red-shifted emission at ∼540 nm compared to **DiKTa**, a small FWHM of 29 nm and delayed lifetime, τ_d, of 4.6 ms and 3.0 ms for **Sym-DiDiKTa** and **Asym-DiDiKTa**, respectively.

Owing to their exciting properties, these compounds were employed as emitters in OLED devices, and to assess improvements in efficiency roll-off, they were also investigated as terminal emitters in hyperfluorescence (HF) OLEDs, which combine a narrowband emitter as terminal dopant with a co-deposited TADF emitter acting as an assistant dopant in a host matrix. Although MR-TADF OLEDs have achieved extremely high EQE$_{max}$, an issue generally encountered is the severe efficiency roll-off that is mainly caused by quenching mechanisms such as singlet–triplet annihilation (STA) and triplet–triplet annihilation (TTA) due to the accumulation of triplet excitons as a result of their typically slow reverse intersystem-crossing rate (k_{RISC}).[17,38] Therefore, a potential solution to circumvent this issue is to use MR-TADF compounds in combination with an efficient exciton harvesting assistant dopant in a HF device.[39–41] In these devices, exciton harvesting is managed by the donor–acceptor TADF assistant dopant and these excitons are transferred to the terminal MR-TADF emitter *via* a Förster resonant energy transfer (FRET) mechanism. Emission from the terminal emitter then occurs, benefiting from the typically fast radiative decay and narrowband emission of the MR-TADF compound.[39] To ensure efficient FRET, there must be an effective overlap between the emission spectrum of the assistant dopant and the absorption spectrum of the emitter.

Results and discussion

The two emitters were obtained *via* a four-step linear sequence (Fig. 2a). Compound **1** was obtained in good yield following a copper-catalysed Ullman coupling between the previously reported dimethyl 2,5-bis((4-(*tert*-butyl)phenyl)amino)terephthalate[43] and methyl 2-iodobenzoate. Quantitative saponification yielded the key intermediate **2**, which then underwent a four-fold intramolecular Friedel–Crafts acylation of the *in situ*-prepared acyl chloride derivative in the presence of the Lewis acid AlCl$_3$ to afford a mixture of two isomers, **Sym-DiDiKTa** and **Asym-DiDiKTa**, in 36% and 5% yield, respectively, after isolation by column chromatography. The compounds were further purified by gradient-temperature vacuum sublimation and their structure and purity were confirmed by a combination of NMR spectroscopy, high-resolution mass spectrometry, melting point determination and HPLC and elemental analysis.
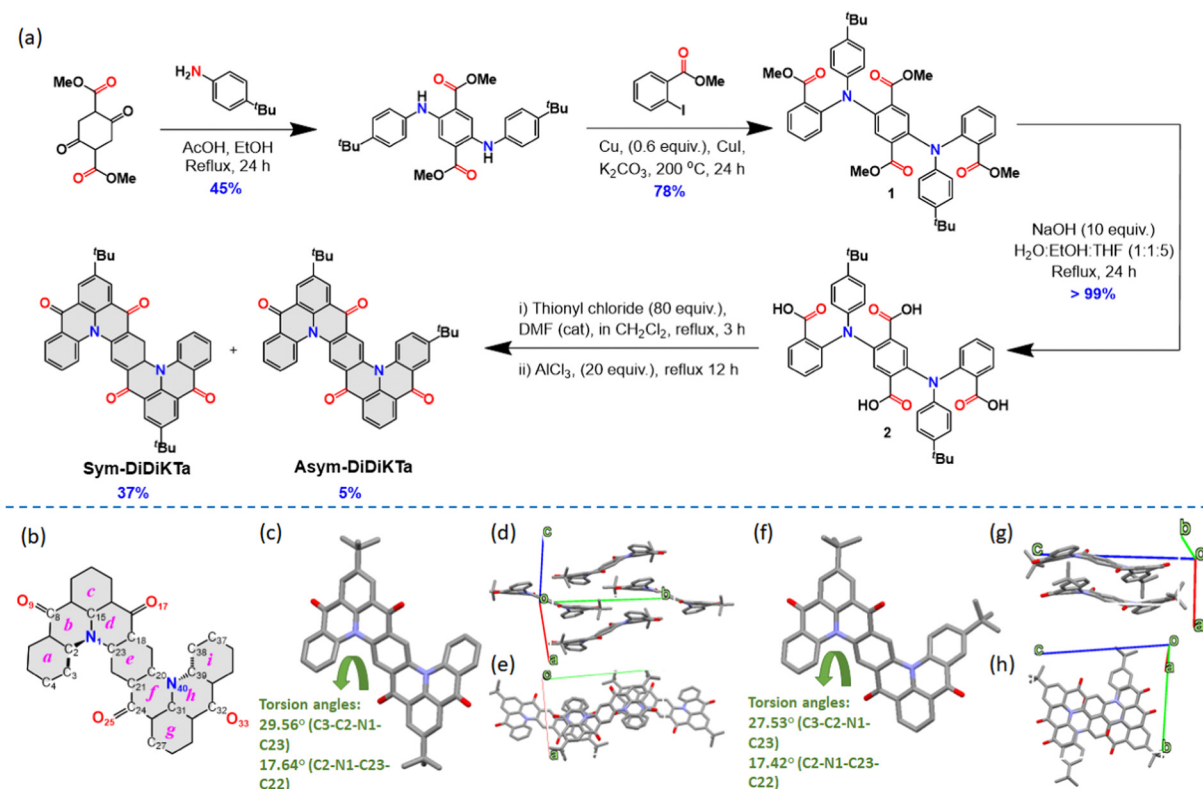

Fig. 2 (a) Synthesis of **Sym-DiDiKTa** and **Asym-DiDiKTa**. (b) Schematic of molecular structure of **Sym-DiDiKTa** and **Asym-DiDiKTa** showing atom labels (double bonds omitted for clarity). (c and f) View showing **Sym-DiDiKTa** and **Asym-DiDiKTa** in the crystal structure (diagonal view). (d and g) Side view of the packing diagram of **Sym-DiDiKTa** and **Asym-DiDiKTa**. (e and h) Top view of the packing diagram of **Sym-DiDiKTa** and **Asym-DiDiKTa**.

This journal is © The Royal Society of Chemistry 2023

J. Mater. Chem. C, 2023, **11**, 8263–8273 | **8265**

Single crystals were isolated following the gradient-temperature vacuum sublimation. Crystallographic data of **Sym-DiDiKTa** and **Asym-DiDiKTa** revealed that both molecules display very similar structures with each **DiKTa** unit showing a helical-like structure. The torsion angles generated by this helical section are similar (torsion angles C3–C2–N1–C23): 29.6(5)° for **Sym-DiDiKTa** and 27.9(3) and 28.1(3)° for **Asym-DiDiKTa** (Fig. 2c and f). Both compounds pack following a one-dimensional slipped π–π stacking motif with inter-planar chains along the c-axis for **Sym-DiDiKTa** [centroid⋯centroid distance 3.5876(18) Å] and along the a-axis for **Asym-DiDiKTa** [centroid⋯centroid distances 3.4697(13)–3.7685(13) Å]. The disposition of the tert-butyl groups in the compounds influences their packing. In the case of **Sym-DiDiKTa**, adjacent molecules are partially superimposed, forming π-stacked chain along the c-axis with the molecules stacked in a slipped manner (Fig. 2d and e). In contrast, for **Asym-DiDiKTa**, adjacent molecules display a greater degree of overlap and more π-stacking (Fig. 2g), resulting in symmetric pairs of adjacent molecules with the tert-butyl groups pointing in the opposite direction (Fig. 2h). Additional π-stacking interactions link these to form π-stacked chains along the a-axis. The distance between the central ring (e) between two nearest molecules is 9.1422(9) Å for **Sym-DiDiKTa**, whereas for **Asym-DiDiKTa** it is only 3.4699(17) Å. We also obtained single crystals of **Sym-DiDiKTa** from slow evaporation of a CH_2Cl_2:MeOH solution (8:2 ratio). Under these conditions, the crystal structure is comprised π-stacked columns of molecules along the crystallographic a-axis (Fig. S13a and b, ESI‡), with greater superimposition than in the previous case (distance between the central rings (e) of 3.8500(2) Å). This is achieved with the aid of MeOH molecules forming both strong and weak hydrogen bonds between and within the columns.

We have previously demonstrated that DFT methods are not appropriate for accurately predicting the excited state properties of MR-TADF materials.[44] Explicit inclusion of second-order electronic correlation effects using wavefunction-based methods such as spin component scaling second-order approximate Coupled–Cluster (SCS-CC2) calculations with the cc-pVDZ basis set addresses this problem, resulting in accurate ΔE_{ST} prediction for MR-TADF materials.[45] The two isomers possess identical S_1 and T_1 energies of 2.93 eV and 2.69 eV, respectively, and thus a ΔE_{ST} of 0.24 eV (Fig. 3), which is similar to previously reported ketone-containing MR-TADF materials.[46] Compared to the parent compound **DiKTa** (ΔE_{ST} = 0.27 eV and S_1 = 3.45 eV), there is a modest decrease in ΔE_{ST} and significant stabilization of S_1. The smaller computed ΔE_{ST} in **Sym-DiDiKTa** to **Asym-DiDiKTa** relative to **DiKTa** is due to the increase in the π-conjugation of these materials compared to **DiKTa** resulting in a lowering of the exchange energy, as has been documented in other extended MR-TADF systems, such as **ν-DABNA** and **OAB-ABP-1**.[26,46] The predicted stabilization of S_1 results from the nitrogen atoms being positioned para to each other, which positively reinforce their electron-donating character, as has been previously reported.[18,41] The oscillator strength associated with the S_0–S_1 transition is significant at 0.26 and 0.27 for **Sym-DiDiKTa** and **Asym-DiDiKTa**, respectively. The difference density plots of S_1 and T_1 of each emitter highlight the alternating pattern of increasing and decreasing electronic density on neighbouring atoms that produce the emissive short-range charge transfer (SRCT) excited state, which is characteristic of MR-TADF materials.[46]

Cyclic voltammetry (CV) and differential pulse voltammetry (DPV) recorded in degassed dichloromethane (Fig. 4a and b) document a reversible reduction wave at E_{red} = −0.96 and −0.94 V vs. SCE for **Sym-DiDiKTa** and **Asym-DiDiKTa**, respectively. The oxidation wave of **Sym-DiDiKTa** is more reversible than that of **Asym-DiDiKTa** (both at 1.53 V vs. SCE), revealing the impact of the regiochemistry that the tert-butyl groups play in terms of electrochemical stability. The corresponding HOMO and LUMO levels are nearly identical, at −5.87 eV for both compounds and −3.38 eV for **Sym-DiDiKTa** and −3.40 eV for **Asym-DiDiKTa**, respectively, which align well with the gas-phase DFT calculations at the PBE0/6-31G(d,p) level of theory (−5.94 eV and −2.69 eV, respectively, Table S11 and Fig. S20, ESI‡). The experimentally determined HOMO levels of **Sym-DiDiKTa** and **Asym-DiDiKTa** are similar to that of **DiKTa** (−5.93 eV), while the LUMO levels are significantly stabilized (LUMO of **DiKTa** = −3.11 eV).[15] The electrochemical data are summarized in Table S9 (ESI‡).
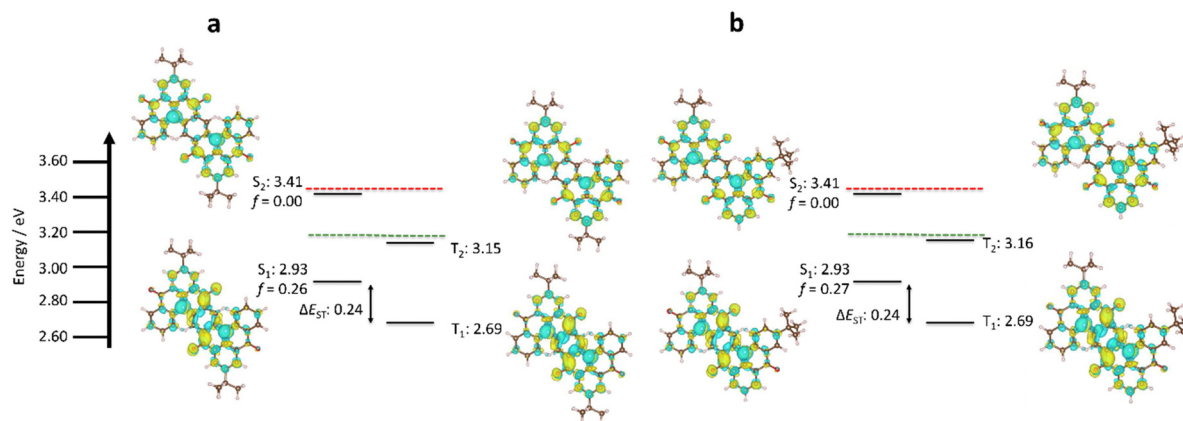

Fig. 3 Difference density picture and excited state energies of **Sym-DiDiKTa** (a) and **Asym-DiDiKTa** (b) calculated at SCS–CC2/cc–pVDZ, where red and green lines indicate S_1 and T_1 energies respectively of **DiKTa**, (isovalue = 0.001).

8266 | J. Mater. Chem. C, 2023, **11**, 8263–8273

This journal is © The Royal Society of Chemistry 2023

The monomolecular photophysical properties of **Sym-DiDiKTa** and **Asym-DiDiKTa** were first studied in dilute toluene solution (Fig. 4c, d and Table 1). The UV-vis absorption spectra of both emitters in toluene are expectedly nearly identical, yet show significant differences compared to that of **DiKTa** in terms of the SRCT absorption band's wavelength (around 435 for **DiKTa**[14,15] but around 515 nm for **Sym-DiDiKTa** and **Asym-DiDiKTa**). The molar absorptivity, ε, of the SRCT band for **Sym-DiDiKTa** and **Asym-DiDiKTa** is 26,325 M^{-1} cm^{-1} and 23,458 M^{-1} cm^{-1}, respectively, assigned to the transition to S_1 according to the SCS-CC2 calculations (Fig. 3). The ε is somewhat larger than reported for **DiKTa** (ε of **DiKTa** = 21 000 M^{-1} cm^{-1}),[15] which is consistent with the trends in the calculated oscillator strength where $f = 0.20$ for **DiKTa**, compared to 0.26 and 0.27 for **Sym-DiDiKTa** and **Asym-DiDiKTa**, respectively. The absorption spectra of both **Sym-DiDiKTa** and **Asym-DiDiKTa** also show a high-energy shoulder at 485 nm ($\varepsilon = 11\,680$ and 10 238 M^{-1} cm^{-1} for **Sym-DiDiKTa** and **Asym-DiDiKTa**, respectively), which likely originates from a vibronic band and not a transition to a higher-lying singlet state given that computed energies of the S_2 state in each of these two compounds is ca. 0.48 eV higher in energy and the S_0–S_2 transition possesses negligible oscillator strength.[16] There is also a high-

energy, high-intensity band at 373 nm ($\varepsilon = 31\,900$ M^{-1} cm^{-1} and 28 527 M^{-1} cm^{-1} for **Sym-DiDiKTa** and **Asym-DiDiKTa**, respectively, Fig. 4c and d), which is assigned to transitions to S_4 and S_5, for **Sym-DiDiKTa** and **Asym-DiDiKTa**, respectively (Table S12, ESI‡) based on the comparison with the SCS-CC2 simulated absorption spectra (Fig. S21 and Table S12, ESI‡). The difference density plots of these states (Fig. S21, ESI‡) show that there is only minimal density situated on the central phenyl ring and more density situated on the carbonyl groups compared with the difference density pattern of the S_1 state (vide supra).

Both compounds display green emission in dilute toluene with emission maxima, λ_{PL}, of 540 nm and 541 nm for **Sym-DiDiKTa** and **Asym-DiDiKTa**, respectively, which are ca. 90 nm red-shifted from that of **DiKTa** ($\lambda_{PL} = 453$ nm). This bathochromic shift is corroborated by the SCS-CC2 calculations.[19,20,31,48] Both compounds display narrow PL spectra at room temperature (FWHM = 29 nm), and small Stokes shifts of ca. 25 nm, which confirms the small degree of geometrical reorganization in the excited state owing to their conformationally rigid structure (Fig. 2c and d). The small degree of positive solvatochromism (Fig. S15 and Tables S2, S3, ESI‡) reflects the SRCT character of the emissive excited state.[15] The S_1 excited state
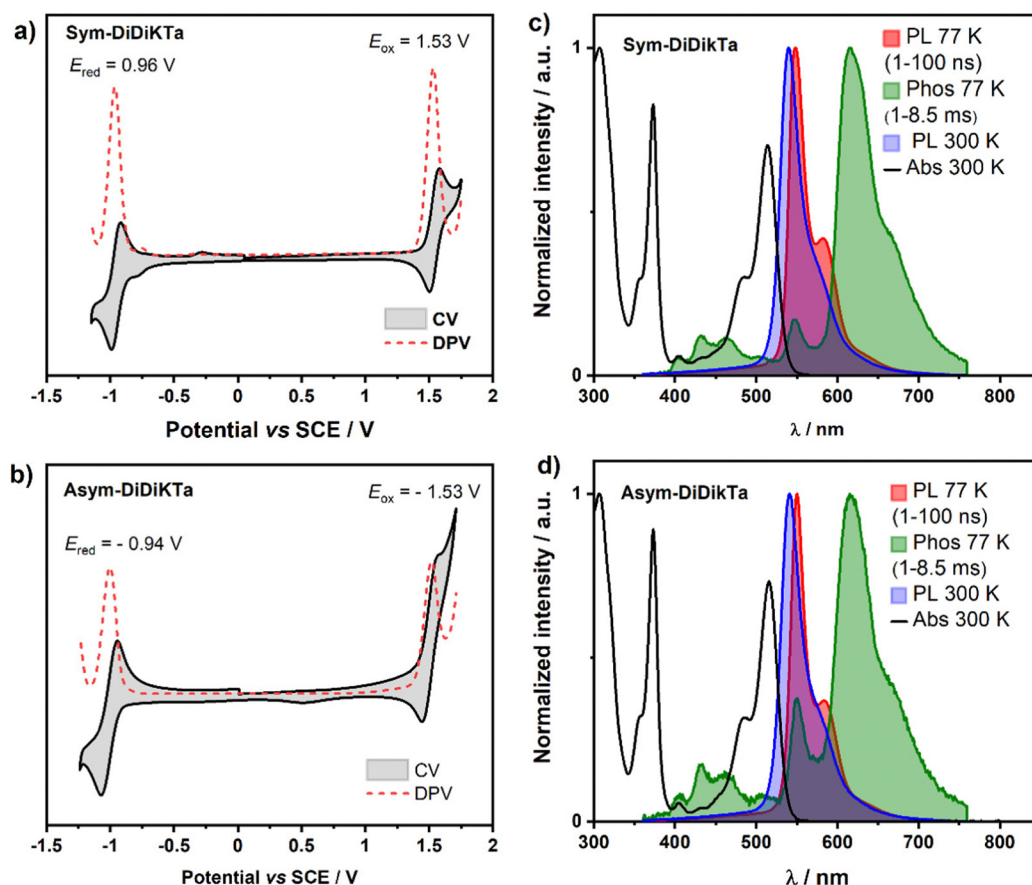

Fig. 4 Optoelectronic characterization of **Sym-DiDiKTa** and **Asym-DiDiKTa**: (a and b) cyclic and differential pulse voltammograms of **Sym-DiDiKTa** and **Asym-DiDiKTa**, respectively, in degassed CH_2Cl_2 with 0.1 M [$^nBu_4N$]PF$_6$ as the supporting electrolyte and Fc/Fc$^+$ as the internal reference (Fc/Fc$^+$ = 0.46 V vs SCE).[47] (c and d) Absorption (black line), steady-state PL spectra obtained in toluene at 300 K (blue line) and 77 K (red line; delay: 1 ns; gate time: 100 ns, λ_{exc} = 343 nm), and phosphorescence (Phos.; delay: 1 ms; gate time: 8.5 ms, λ_{exc} = 343 nm) spectra in toluene glass at 77 K (green olive line) of **Sym-DiDiKTa** and **Asym-DiDiKTa**, respectively.

This journal is © The Royal Society of Chemistry 2023

J. Mater. Chem. C, 2023, **11**, 8263–8273 | **8267**

Table 1 Optoelectronic properties of **Sym-DiDiKTa** and **Asym-DiDiKTa**

	In toluene								In film		
	$\lambda_{abs}{}^{a}$/nm	ε^{a}/M^{-1} cm^{-1}	$\lambda_{PL}{}^{b}$/nm	Φ_{PL} in N$_2$ (air)^{c}/%	FWHM^{d}/ nm (eV)	$S_1{}^{e}$/eV	$T_1{}^{e}$/eV	$\Delta E_{ST}{}^{f}$/eV	λ_{PL}/nm	Φ_{PL}/%	FWHM^{d}/ nm (eV)
Sym-DiDiKTa	373/485/515	31900/11680/26325	540	69 (65)	29 (0.12)	2.26	2.02	0.24	542^{g}	64	35 (0.14)^{g}
Asym-DiDiKTa	373/485/516	28527/10238/23458	541	53 (50)	29 (0.12)	2.25	2.02	0.23	547^{g}	57	35 (0.14)^{g}

^{a} UV–vis absorption of CT transition. ^{b} Prompt emission in toluene degassing with N$_2$. ^{c} Photoluminescence quantum yield in toluene relative to quinine sulfate in 1N H$_2$SO$_4$ (Φ_{PL} = 54.6%) ^{d} Full-width at half-maximum. ^{e} Obtained using an integrating sphere under N$_2$. ^{f} Energy gap between S_1 and T_1 calculated from the difference of the peaks of the fluorescence and phosphorescence spectra in toluene glass at 77 K. ^{g} 1 wt% **Sym-DiDiKTa** and **Asym-DiDiKTa** doped in mCP.

energy levels were determined to be 2.26 and 2.25 eV, respectively, for **Sym-DiDiKTa** and **Asym-DiDiKTa** and the T_1 excited state energy levels are identical at 2.02 eV, each obtained from the λ_{PL} of the respective prompt fluorescence and phosphorescence spectra in toluene glass at 77 K. We note that the nature of T_1 and S_1 are identical based on the difference density plots (Fig. 3). The corresponding ΔE_{ST} values are 0.24 eV and 0.23 eV, respectively, for **Sym-DiDiKTa** and **Asym-DiDiKTa**. These values match with those predicted by SCS-CC2 calculations (ΔE_{ST} = 0.24 eV for both compounds). The PL quantum yield, Φ_{PL}, in toluene is 70% under N$_2$, which decreases to 64% in air for **Sym-DiDiKTa** and 53% under N$_2$ and 50% in air for **Asym-DiDiKTa**. The Φ_{PL} values were next measured for vacuum-deposited 1 wt% doped thin films in 1,3-bis(N-carbazolyl)benzene (mCP). The Φ_{PL} values were determined to be 64% and 57% for **Sym-DiDiKTa** and **Asym-DiDiKTa**, respectively (Table S5, ESI‡). The Φ_{PL} values closely resemble those obtained in dilute toluene, which implies that non-

radiative decay due to vibrations is not significant in these compounds.

We next investigated the solid-state photophysical properties of spin-coated 1 wt% **Sym-DiDiKTa** and **Asym-DiDiKTa** doped thin films in mCP. The low doping concentration was selected to mitigate the potential for undesired aggregation in the films. As shown in Fig. 5a and c, at 300 K, **Sym-DiDiKTa** and **Asym-DiDiKTa** show a similar emission profile with λ_{PL} at 542 and 547 nm, respectively, values that are close to the prompt emission maximum in toluene. A small FWHM of 35 nm (0.13 eV) was calculated for both compounds in the films, which is slightly broader than the FWHM of 29 nm (0.12 eV) determined in toluene, indicating the influence of the matrix on the conformational stabilization of the excited states. Another aspect to consider are concentration-dependent aggregation effects since the concentration of emitters at 1 wt% doping in the film is higher than that of the 10^6 M solution.
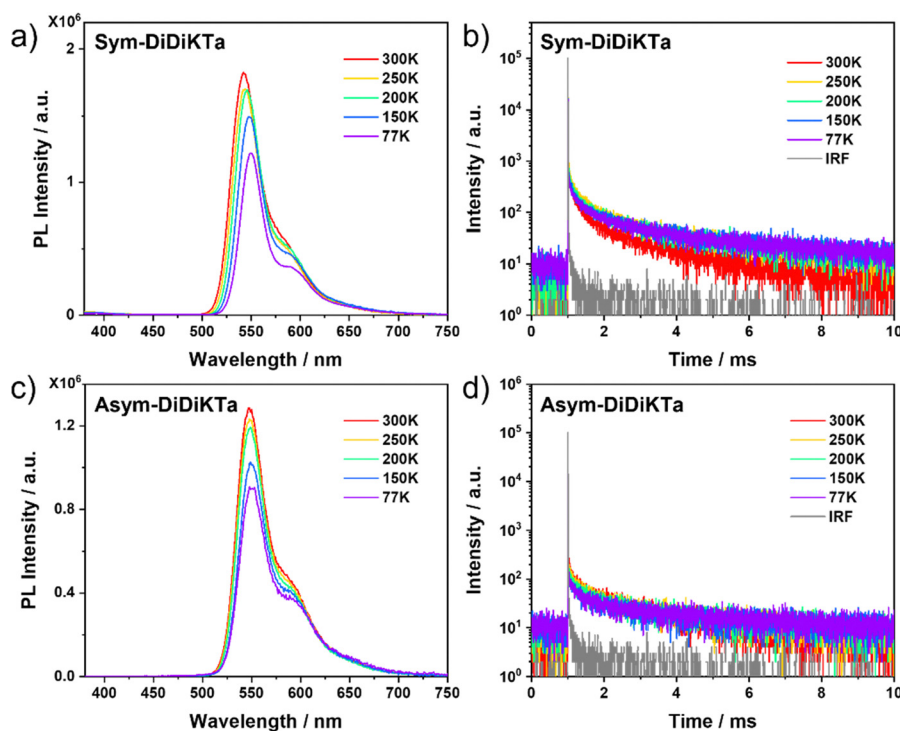

Fig. 5 (a and c) Temperature-dependent PL study of 1 wt% of **Sym-DiDiKTa** and **Asym-DiDiKTa**, respectively, in mCP, λ_{exc} = 350 nm. (b and d) Temperature-dependent time-resolved PL decays for 1 wt% **Sym-DiDiKTa** and **Asym-DiDiKTa**, respectively, in mCP matrix (λ_{exc} = 378 nm).

8268 | J. Mater. Chem. C, 2023, 11, 8263–8273

This journal is © The Royal Society of Chemistry 2023

The average τ_d values are 4.6 ms and 3.0 ms for **Sym-DiDiKTa** and **Asym-DiDiKTa**, respectively (Fig. 5 and Table S7, ESI‡). We then compared the oxygen dependence of the PL spectrum at room temperature. The PL spectrum in air shows a small decrease in intensity compared to the spectrum under vacuum (Fig. S17a and b, ESI‡), indicating a weak involvement of triplet excited states. The temperature-dependent PL spectra (Fig. 5a and c) and temperature-dependent time-resolved PL decays (Fig. 5b and d) of both emitters document the characteristic decrease in intensity and in the contribution of the delayed emission, respectively, with decreasing temperature. This could be due to the MR-TADF behavior only being apparent in a suitable host matrix due to exciplex-like host-emitter interactions.[29]

OLED characterization

We fabricated vacuum-deposited OLEDs using **Sym-DiDiKTa** and **Asym-DiDiKTa** as the emitters. The following device configuration was used: indium tin oxide (ITO)-coated glass (100 nm)/TAPC (35 nm)/TCTA (10 nm)/mCP: 3 wt% of **Sym-DiDiKTa** or **Asym-DiDiKTa** (20 nm)/TmPyPB (30 nm)/Liq (2 nm)/Al (100 nm). 1,1-Bis[[di-4-tolylamino)phenyl]cyclohexane (TAPC) is the hole-transporting layer, 4,4′,4-tris(carbazol-9-yl)triphenylamine (TCTA) is used for electron-blocking and host layers, 1,3,5-tris(3-pyridyl-3-phenyl)benzene (TmPyPB) is the electron-transporting layer, and lithium 8-hydroxyquinolinolate (Liq) and aluminum are the electron injection and cathode layers, respectively. Fig. 6 and Table 2 summarize all the device characteristics. TADF-only devices based on **Sym-DiDiKTa** (Device **I**) and **Asym-DiDiKTa** (Device **II**) emitted green narrow-band electroluminescence, λ_{EL}, at 543 and 544 nm, respectively, values that are consistent to their corresponding λ_{PL}. The FWHMs of both Devices **I** and **II** are 36 nm, which resulted in CIE coordinates of (0.362, 0.623) and (0.376, 0.613), respectively. The EQE$_{max}$ of Device **I** is 9.8%, which is slightly lower than the 10.5% measured for Device **II**. We hypothesized that the moderate Φ_{PL} in the mCP-doped films limits the EQE$_{max}$ values in Devices **I** and **II**. The moderate Φ_{PL} may be due to the long-lived delayed fluorescence that permits a greater probability that non-

radiative decay processes such as triplet-polaron quenching and triplet–triplet annihilation will contribute to the decay of the excitons. Both devices suffered from severe efficiency roll-off issues, which in part are due to the long delayed fluorescence lifetimes of **Sym-DiDiKTa** and **Asym-DiDiKTa**. Moreover, the linear decrease in the EQE – current density curve indicates possible exciton-polaron annihilation processes, which can be ascribed to trap formation by the emitters.

To improve the device performance, we implemented a hyperfluorescence (HF) strategy in Device **III** with the following device structure: indium tin oxide (ITO)-coated glass (100 nm)/HAT-CN (10 nm)/Tris-PCz (30 nm)/mCBP (5 nm)/mCBP: 20 wt% 4CzIPN: 3 wt% **Asym-DiDiKTa** (30 nm)/T2T (10 nm)/BPy-TP2 (40 nm)/Liq (2 nm)/Al (100 nm), where 1,4,5,8,9,11-hexaazatri-phenyl-enehexacarbonitrile (HAT-CN) is the hole-injection layer, 9-phenyl-3,6-bis(9-phenyl-9*H*carbazol-3-yl)-9*H*-carbazole (Tris-PCz) is the hole-transporting layer, mCBP is used in the exciton-blocking and host layers, 1,2,3,5-tetrakis(carbazol-9-yl)-4,6-dicyanobenzene (4CzIPN) is a green TADF assistant dopant, 2,4,6-tris(biphenyl-3-yl)-1,3,5-triazine (T2T) is the hole-blocking layer and 2,7-di(2,2′-bipyridin-5-yl)triphenylene (BPy-TP2) is the electron-transporting layer, and lithium 8-hydroxyquinolinolate (Liq) and Al are the electron injection and cathode layers, respectively. Gratifyingly, the device performance improved and an EQE$_{max}$ of 19.9% was achieved along with an enhanced maximum brightness of 53625 cd m^{-2}. The HF device not only resulted in a better EQE, but also reduced the efficiency roll-off when compared to Device **II**. The λ_{EL} is red-shifted to 548 nm and there is a slightly larger FWHM of 56 nm. The broader FWHM may originate from an incomplete energy transfer from 4CzIPN to **Asym-DiDiKTa**.

LEC devices

The light-emitting electrochemical cell (LEC) can be comprised of solely air-stable materials and feature a very simple and robust device structure in the form of a single-layer active material sandwiched between two electrodes. This renders the LEC technology highly fit for scalable and cost-efficient printing and coating fabrication under ambient air.[49,50] The characteristic feature
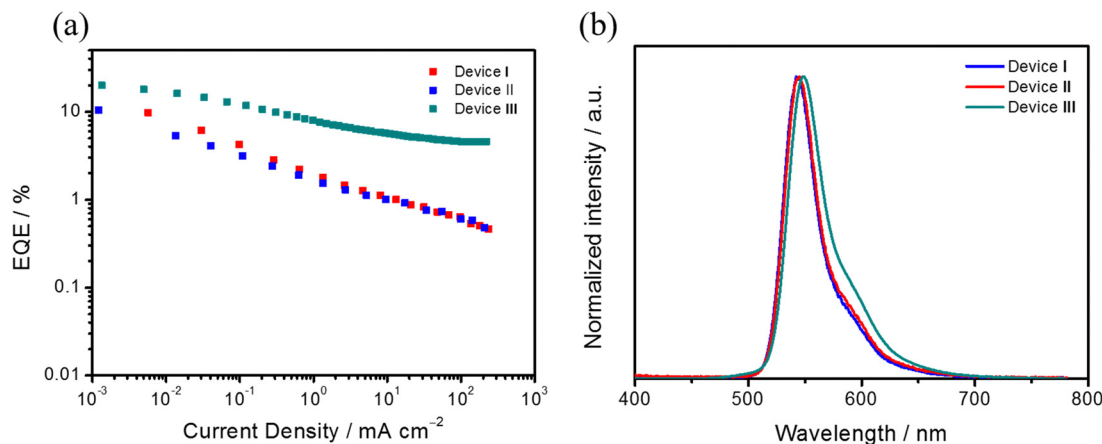

Fig. 6 (a) EQE *versus* current density curves of Devices **I**–**III**. (b) Electroluminescence spectra of Devices **I**–**III** at 500 cd m^{-2}.

This journal is © The Royal Society of Chemistry 2023

J. Mater. Chem. C, 2023, **11**, 8263–8273 | **8269**

Table 2 Summary of device characteristics

Device	Dopant	V_{on}/V^a	EQE/%[b]	λ_{EL}/nm^c	Max. brightness (cd m^{-2})[d]	FWHM/nm[c]	CIE (x, y)[c]
I	3 wt% **Sym-DiDiKTa**	3.5	9.8/1.8/0.8	543	4310	36	(0.359, 0.624)
II	3 wt% **Asym-DiDiKTa**	4	10.5/1.3/0.8	544	3989	36	(0.369, 0.616)
III	3 wt% **Asym-DiDiKTa**: 20 wt% **4CzIPN**	3.2	19.9/9.9/6.4	548	53625	56	(0.397, 0.592)

[a] Voltage at 1 cd m^{-2}. [b] Value at maximum, 100 cd m^{-2} and 1000 cd m^{-2}. [c] Value at 500 cd m^{-2}. [d] Maximum brightness.

of LEC devices is the combination of mobile ions with the emissive organic semiconductor within the emissive layer.[51,52] These mobile ions redistribute when a voltage is applied, and enable p-type electrochemical doping of the organic semiconductor at the anode and n-type doping at the cathode. With time, these doping regions grow in size and make contact under the formation of a p–n junction. The fact that **Sym-DiDiKTa** displays highly reversible electrochemical oxidation and reduction behaviour in the cyclic voltammetry experiments (Fig. 4a) suggests that it could be fit for the task of the emissive organic semiconductor in a LEC device.

We fabricated and characterized LEC devices with the following configuration: indium tin oxide (140 nm)/poly(3,4-ethylenedioxythiophene) polystyrene sulfonate (40 nm)/26DCzPPy (44 wt%): POT2T (44 wt%):**Sym-DiDiKTa** (4 wt%):THABF$_4$ (8 wt%) (100 nm)/ Al (100 nm), where THABF$_4$ (tetrahexylammonium tetrafluoroborate) is the ionic liquid electrolyte that contributes the mobile ions, and 6-bis(3-carbazol-9-yl)pyridine (26DCzPPy):(1,3,5-triazine-2,4,6-triyl)tris(benzene-3,1-diyl)tris(diphenylphosphine oxide) (POT2T) is a blend-host matrix, which was introduced to enable for the formation of a uniform solution-processed thin film and to suppress losses by exciton-polaron[53] and exciton-exciton quenching.

Fig. 7a presents the steady-state EL spectrum recorded during the driving with a constant current density of 77 mA cm^{-2}, with the λ_{EL} at 551 nm and the FWHM being 60 nm. The broadening of the EL spectrum of the LEC device in comparison to the PL spectra in Fig. 5a indicates the formation of exciplexes with the blend host. This conclusion is supported by the fact that the FWHM of the EL spectrum is essentially independent of the guest concentration

for a guest concentration range of 1 to 8 wt% (Fig. S22, ESI‡). Fig. 7b details the voltage and luminance transients recorded during the early stages of the constant-current driving. The observed initial decrease of the voltage is a characteristic indicator of conductivity-enhancing electrochemical doping, whereas the increase in luminance is in line with the gradual formation of a p-n junction, where electrons and holes can recombine efficiently into excitons. Importantly, these observations imply that the **Sym-DiDiKTa** emitter can be *in situ* electrochemically p- and n-type doped during LEC operation. This conclusion is further supported by the fact that the LEC device delivered a significant luminance of 300 cd m^{-2} despite being equipped with an air-stable Al cathode in direct contact with the active emissive material. Finally, the luminance turn-on time is a direct indicator of the ion mobility in the active material,[54,55] and the comparatively fast turn-on time of less than 2 s to 100 cd m^{-2} demonstrates that the ion mobility in the active material is high.

Conclusion

In summary, new amine/carbonyl-based MR-TADF materials were developed by an approach that expands the π-conjugated backbone to show green-yellow emission. The regio-functionalization of the *tert*-butyl groups was shown to significantly impact the single-crystal packing structure. With a ΔE_{ST} of around 0.23 eV in toluene, the narrowband emitters, FWHM, of 29 nm, display TADF activity with a τ_d of 4.6 ms and 3.0 ms for **Sym-DiDiKTa** and **Asym-DiDiKTa**, respectively. Application
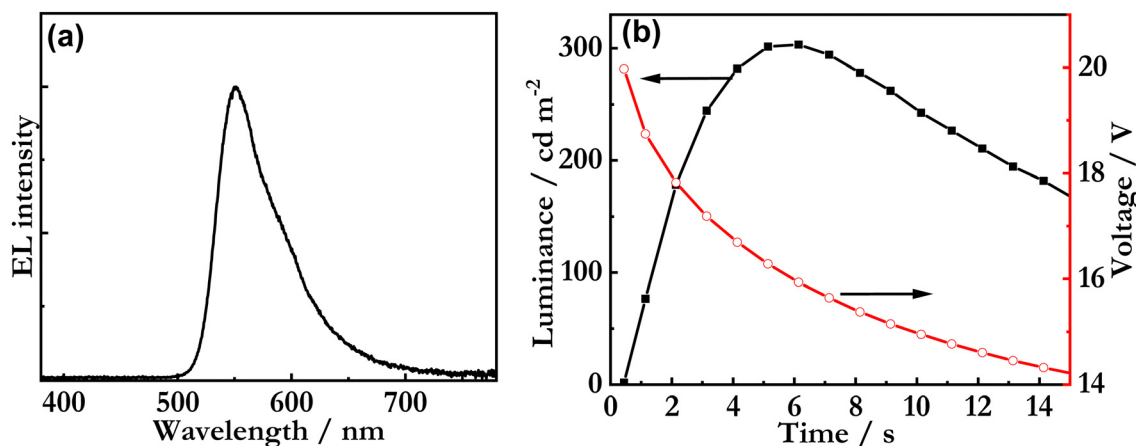

Fig. 7 (a) The steady-state EL spectrum. (b) The temporal evolution of the luminance (left y-axis, solid black squares) and the drive voltage (right y-axis, open red circles) for the ITO/PEDOT:PSS/26DCzPPy:POT2T: **Sym-DiDiKTa**:THABF$_4$/Al LEC device. The LEC devices were driven by a constant current density of 77 mA cm^{-2}.

8270 | *J. Mater. Chem. C*, 2023, **11**, 8263–8273

This journal is © The Royal Society of Chemistry 2023

in OLEDs provided devices with electroluminescence maxima at around 544 nm, and an EQE_{max} of *circa* 10% which low value is attributed to the long delayed lifetimes of this class. Upon further studies in hyperfluorescence devices, an EQE of 19.9% was finally obtained, showing the promise of this class of molecules towards this strategy. We also show the first examples of a LEC device incorporating an MR-TADF emitter. With a λ_{EL} at 551 nm and a larger FWHM of 60 nm due to formation of exciplexes with the host, the device based on **Sym-DiDiKTa** delivered a significant luminance of 300 cd m^{-2} and high ion mobility with a fast turn-on time of less than 2 s to 100 cd m^{-2}.

Conflicts of interest

The authors declare that they have no conflict of interest.

Acknowledgements

References

1 X. K. Chen, D. Kim and J. L. Brédas, Thermally Activated Delayed Fluorescence (TADF) Path toward Efficient Electroluminescence in Purely Organic Materials: Molecular Level Insight, *Acc. Chem. Res.*, 2018, **51**(9), 2215–2224.

2 T. Tsujimura, *OLED display fundamentals and applications*, 2017.

3 H. Uoyama, K. Goushi, K. Shizu, H. Nomura and C. Adachi, Highly efficient organic light-emitting diodes from delayed fluorescence, *Nature*, 2012, **492**(7428), 234–238.

4 G. Méhes, H. Nomura, Q. Zhang, T. Nakagawa and C. Adachi, Enhanced electroluminescence efficiency in a spiro-acridine derivative through thermally activated delayed fluorescence, *Angew. Chem., Int. Ed.*, 2012, **51**(45), 11311–11315.

5 T. Nakagawa, S. Y. Ku, K. T. Wong and C. Adachi, Electroluminescence based on thermally activated delayed fluorescence generated by a spirobifluorene donor-acceptor structure, *Chem. Commun.*, 2012, **48**(77), 9580–9582.

6 S. Hirata, Y. Sakai, K. Masui, H. Tanaka, S. Y. Lee, H. Nomura, N. Nakamura, M. Yasumatsu, H. Nakanotani, Q. Zhang, K. Shizu, H. Miyazaki and C. Adachi, Highly efficient blue electroluminescence based on thermally activated delayed fluorescence, *Nat. Mater.*, 2015, **14**(3), 330–336.

7 M. Y. Wong and E. Zysman-Colman, Purely Organic Thermally Activated Delayed Fluorescence Materials for Organic Light-Emitting Diodes, *Adv. Mater.*, 2017, **29**(22), 1–54.

8 A. Endo, M. Ogasawara, A. Takahashi, D. Yokoyama, Y. Kato and C. Adachi, Thermally activated delayed fluorescence from Sn^{4+}-porphyrin complexes and their application to organic light-emitting diodes -A novel mechanism for electroluminescence, *Adv. Mater.*, 2009, **21**(47), 4802–4806.

9 A. Endo, K. Sato, K. Yoshimura, T. Kai, A. Kawada, H. Miyazaki and C. Adachi, Efficient up-conversion of triplet excitons into a singlet state and its application for organic light emitting diodes, *Appl. Phys. Lett.*, 2011, **98**(8), 2011–2014.

10 C. A. Parker and C. G. Hatchard, Triplet–singlet emission in fluid solutions, *Trans. Faraday Soc.*, 1961, **57**, 1894–1904.

11 F. Santoro, A. Lami, R. Improta, J. Bloino and V. Barone, Effective method for the computation of optical spectra of large molecules at finite temperature including the Duschinsky and Herzberg-Teller effect: The Qx band of porphyrin as a case study, *J. Chem. Phys.*, 2008, **128**(22), 224311.

12 X. Qiu, G. Tian, C. Lin, Y. Pan, X. Ye, B. Wang, D. Ma, D. Hu, Y. Luo and Y. Ma, Narrowband Emission from Organic Fluorescent Emitters with Dominant Low-Frequency Vibronic Coupling, *Adv. Opt. Mater.*, 2020, **9**(4), 2001845.

13 H. W. Chen, J. H. Lee, B. Y. Lin, S. Chen and S. T. Wu, Liquid crystal display and organic light-emitting diode display: present status and future perspectives, *Light: Sci. Appl.*, 2018, **7**(3), 17168.

14 Y. Yuan, X. Tang, X. Y. Du, Y. Hu, Y. J. Yu, Z. Q. Jiang, L. S. Liao and S. T. Lee, The Design of Fused Amine/Carbonyl System for Efficient Thermally Activated Delayed Fluorescence: Novel Multiple Resonance Core and Electron Acceptor, *Adv. Opt. Mater.*, 2019, **7**(7), 1801536.

15 D. Hall, S. M. Suresh, P. L. dos Santos, E. Duda, S. Bagnich, A. Pershin, P. Rajamalli, D. B. Cordes, A. M. Z. Slawin, D. Beljonne, A. Köhler, I. D. W. Samuel, Y. Olivier and E. Zysman-Colman, Improving Processability and Efficiency of Resonant TADF Emitters: A Design Strategy, *Adv. Opt. Mater.*, 2020, **8**(2), 1901627.

16 X. Li, Y. Z. Shi, K. Wang, M. Zhang, C. J. Zheng, D. M. Sun, G. L. Dai, X. C. Fan, D. Q. Wang, W. Liu, Y. Q. Li, J. Yu, X. M. Ou, C. Adachi and X. H. Zhang, Thermally Activated Delayed Fluorescence Carbonyl Derivatives for Organic Light-Emitting Diodes with Extremely Narrow Full Width at Half-Maximum, *ACS Appl. Mater. Interfaces*, 2019, **11**(14), 13472–13480.

17 S.-n Zou, C.-c Peng, S.-y Yang, Y.-k Qu, Y.-j Yu, X. Chen, Z.-q Jiang and L.-s Liao, Fully Bridged Triphenylamine Derivatives as Color-Tunable Thermally Activated Delayed Fluorescence Emitters, *Org. Lett.*, 2021, **23**(3), 958–962.

18 Y. Tsuchiya, Y. Ishikawa, S. H. Lee, X. K. Chen, J. L. Brédas, H. Nakanotani and C. Adachi, Thermally Activated Delayed

This journal is © The Royal Society of Chemistry 2023

J. Mater. Chem. C, 2023, **11**, 8263–8273 | 8271

Fluorescence Properties of Trioxoazatriangulene Derivatives Modified with Electron Donating Groups, *Adv. Opt. Mater.*, 2021, **9**(14), 2002174.

19 F. Huang, K. Wang, Y. Z. Shi, X. C. Fan, X. Zhang, J. Yu, C. S. Lee and X. H. Zhang, Approaching Efficient and Narrow RGB Electroluminescence from D-A-Type TADF Emitters Containing an Identical Multiple Resonance Backbone as the Acceptor, *ACS Appl. Mater. Interfaces*, 2021, **13**(30), 36089–36097.

20 Y. Zhang, D. Zhang, T. Huang, A. J. Gillett, Y. Liu, D. Hu, L. Cui, Z. Bin, G. Li, J. Wei and L. Duan, Multi-Resonance Deep-Red Emitters with Shallow Potential-Energy Surfaces to Surpass Energy-Gap Law, *Angew. Chem., Int. Ed.*, 2021, **60**(37), 20498–20503.

21 T. Hatakeyama, K. Shiren, K. Nakajima, S. Nomura, S. Nakatsuka, K. Kinoshita, J. Ni, Y. Ono and T. Ikuta, Ultrapure Blue Thermally Activated Delayed Fluorescence Molecules: Efficient HOMO-LUMO Separation by the Multiple Resonance Effect, *Adv. Mater.*, 2016, **28**(14), 2777–2781.

22 Y. Kondo, K. Yoshiura, S. Kitera, H. Nishi, S. Oda, H. Gotoh, Y. Sasada, M. Yanai and T. Hatakeyama, Narrowband deep-blue organic light-emitting diode featuring an organoboron-based emitter, *Nat. Photonics*, 2019, **13**(10), 678–682.

23 Q. Wang, Y. Xu, T. Yang, J. Xue and Y. Wang, Precise Functionalization of a Multiple-Resonance Framework: Constructing Narrowband Organic Electroluminescent Materials with External Quantum Efficiency over 40, *Adv. Mater.*, 2023, **35**(3), e2205166.

24 Y. Xu, Q. Wang, J. Wei, X. Peng, J. Xue, Z. Wang, S. J. Su and Y. Wang, Constructing Organic Electroluminescent Material with Very High Color Purity and Efficiency Based on Poly-cyclization of the Multiple Resonance Parent Core, *Angew. Chem., Int. Ed.*, 2022, **61**(30), e202204652.

25 Y. Zou, J. Hu, M. Yu, J. Miao, Z. Xie, Y. Qiu, X. Cao and C. Yang, High-Performance Narrowband Pure-Red OLEDs with External Quantum Efficiencies up to 36.1% and Ultra-low Efficiency Roll-Off, *Adv. Mater.*, 2022, **34**(29), 2201442.

26 N. Ikeda, S. Oda, R. Matsumoto, M. Yoshioka, D. Fukushima, K. Yoshiura, N. Yasuda and T. Hatakeyama, Solution-Processable Pure Green Thermally Activated Delayed Fluorescence Emitter Based on the Multiple Resonance Effect, *Adv. Mater.*, 2020, **32**, 2004072.

27 H. Min, I. S. Park and T. Yasuda, *cis*-Quinacridone-Based Delayed Fluorescence Emitters: Seemingly Old but Renewed Functional Luminogens, *Angew. Chem., Int. Ed.*, 2021, **60**(14), 7643–7648.

28 S. Wu, A. K. Gupta, K. Yoshida, J. Gong, D. Hall, D. B. Cordes, A. M. Z. Slawin, I. D. W. Samuel and E. Zysman-Colman, Highly Efficient Green & Red Narrowband Emissive Organic Light-Emitting Diodes Employing Multi-Resonant Thermally Activated Delayed Fluorescence Emitters, *Angew. Chem., Int. Ed.*, 2022, **61**(52), e202213697.

29 X. Wu, B. K. Su, D. G. Chen, D. Liu, C. C. Wu, Z. X. Huang, T. C. Lin, C. H. Wu, M. Zhu, E. Y. Li, W. Y. Hung, W. Zhu and P. T. Chou, The role of host–guest interactions in organic emitters employing MR-TADF, *Nat. Photonics*, 2021, **15**(10), 780–786.

30 S. Madayanad Suresh, D. Hall, D. Beljonne, Y. Olivier and E. Zysman-Colman, Multiresonant Thermally Activated Delayed Fluorescence Emitters Based on Heteroatom-Doped Nanographenes: Recent Advances and Prospects for Organic Light-Emitting Diodes, *Adv. Funct. Mater.*, 2020, **30**(33), 1908677.

31 M. Yang, I. S. Park and T. Yasuda, Full-Color, Narrowband, and High-Efficiency Electroluminescence from Boron and Carbazole Embedded Polycyclic Heteroaromatics, *J. Am. Chem. Soc.*, 2020, **142**(46), 19468–19472.

32 D. Sun, M. Suresh, D. Hall, M. Zhang, C. Si, D. B. Cordes, A. M. Z. Slawin, Y. Olivier, X. Zhang and E. Zysman-colman, The design of an extended multiple resonance TADF emitter based on a polycyclic amine/carbonyl system, *Mater. Chem. Front.*, 2020, **4**, 2018–2022.

33 S. Wu, W. Li, K. Yoshida, D. Hall, S. Madayanad Suresh, T. Sayner, J. Gong, D. Beljonne, Y. Olivier, I. D. W. Samuel and E. Zysman-Colman, Excited-State Modulation in Donor-Substituted Multiresonant Thermally Activated Delayed Fluorescence Emitters, *ACS Appl. Mater. Interfaces*, 2022, **14**(19), 22341–22352.

34 J. M. dos Santos, D. Sun, J. M. Moreno-Naranjo, D. Hall, F. Zinna, S. T. J. Ryan, W. Shi, T. Matulaitis, D. B. Cordes, A. M. Z. Slawin, D. Beljonne, S. L. Warriner, Y. Olivier, M. J. Fuchter and E. Zysman-Colman, An S-shaped double helicene showing both multi-resonance thermally activated delayed fluorescence and circularly polarized luminescence, *J. Mater. Chem. C*, 2022, **10**, 4861–4870.

35 X. Lv, J. Miao, M. Liu, Q. Peng, C. Zhong, Y. Hu, X. Cao, H. Wu, Y. Yang, C. Zhou, J. Ma, Y. Zou and C. Yang, Extending the π-Skeleton of Multi-Resonance TADF Materials towards High-Efficiency Narrowband Deep-Blue Emission, *Angew. Chem., Int. Ed.*, 2022, **61**(29), e202201588.

36 X. Cai, J. Xue, C. Li, B. Liang, A. Ying, Y. Tan, S. Gong and Y. Wang, Achieving 37.1% Green Electroluminescent Efficiency and 0.09 eV Full Width at Half Maximum Based on a Ternary Boron-Oxygen-Nitrogen Embedded Polycyclic Aromatic System, *Angew. Chem., Int. Ed.*, 2022, **61**(23), e202200337.

37 X. F. Luo, H. X. Ni, A. Q. Lv, X. K. Yao, H. L. Ma and Y. X. Zheng, High-Efficiency and Narrowband OLEDs from Blue to Yellow with Ternary Boron/Nitrogen-Based Polycyclic Heteroaromatic Emitters, *Adv. Opt. Mater.*, 2022, **10**(16), 2200504.

38 Y. Zhang, D. Zhang, J. Wei, Z. Liu, Y. Lu and L. Duan, Multi-Resonance Induced Thermally Activated Delayed Fluorophores for Narrowband Green OLEDs, *Angew. Chem., Int. Ed.*, 2019, **58**(47), 16912–16917.

39 Y. Zhang, J. Wei, D. Zhang, C. Yin, G. Li, Z. Liu, X. Jia, J. Qiao and L. Duan, Sterically Wrapped Multiple Resonance Fluor-ophors for Suppression of Concentration Quenching and Spectrum Broadening, *Angew. Chem., Int. Ed.*, 2021, **61**(2), 202113206.

40 C. Y. Chan, M. Tanaka, Y. T. Lee, Y. W. Wong, H. Nakanotani, T. Hatakeyama and C. Adachi, Stable pure-blue hyperfluorescence organic light-emitting diodes with

8272 | *J. Mater. Chem. C*, 2023, **11**, 8263–8273

This journal is © The Royal Society of Chemistry 2023

high-efficiency and narrow emission, *Nat. Photonics*, 2021, **15**(3), 203–207.

41 J. Wei, C. Zhang, D. Zhang, Y. Zhang, Z. Liu, Z. Li, G. Yu and L. Duan, Indolo[3,2,1-jk]carbazole Embedded Multiple-Resonance Fluorophors for Narrowband Deep-blue Electroluminescence with EQE ≈ 34.7% and CIEy ≈ 0.085, *Angew. Chem., Int. Ed.*, 2021, **60**(22), 12269–12273.

42 J. J. C. Lee, C. Chi and J. Wu, Synthesis of a Highly Fluorescent Bis(1,4-oxaborine)pentacene, *ChemPlusChem*, 2021, **86**(6), 836–839.

43 M. Shimizu, Y. Asai, Y. Takeda, A. Yamatani and T. Hiyama, Twisting strategy applied to N,N-diorganoquinacridones leads to organic chromophores exhibiting efficient solid-state fluorescence, *Tetrahedron Lett.*, 2011, **52**(32), 4084–4089.

44 A. Pershin, D. Hall, V. Lemaur, J. C. Sancho-Garcia, L. Muccioli, E. Zysman-Colman, D. Beljonne and Y. Olivier, Highly emissive excitons with reduced exchange energy in thermally activated delayed fluorescent molecules, *Nat. Commun.*, 2019, **10**(1), 597.

45 D. Hall, K. Stavrou, E. Duda, A. Danos, S. Bagnich, S. Warriner, A. M. Z. Slawin, D. Beljonne, A. Köhler, A. Monkman, Y. Olivier and E. Zysman-Colman, Diindolocarbazole – achieving multiresonant thermally activated delayed fluorescence without the need for acceptor units, *Mater. Horiz.*, 2022, **9**, 1068–1080.

46 D. Hall, J. Carlos Sancho-Garcia, A. Pershin, D. Beljonne, E. Zysman-Colman and Y. Olivier, Modelling of multi-resonant thermally activated delayed fluorescence emitters-properly accounting for electron correlation is key!, *J. Chem. Theory Comput.*, 2022, **18**(8), 4903–4918.

47 N. G. Connelly and W. E. Geiger, Chemical redox agents for organometallic chemistry, *Chem. Rev.*, 1996, **96**(2), 877–910.

48 M. Yang, S. Shikita, H. Min, I. S. Park, H. Shibata, N. Amanokura and T. Yasuda, Wide-Range Color Tuning of Narrowband Emission in Multi-resonance Organoboron Delayed Fluorescence Materials through Rational Imine/Amine Functionalization, *Angew. Chem., Int. Ed.*, 2021, **60**(43), 23142–23147.

49 A. Sandström, H. F. Dam, F. C. Krebs and L. Edman, Ambient fabrication of flexible and large-area organic light-emitting devices using slot-die coating, *Nat. Commun.*, 2012, **3**, 1002.

50 G. Hernandez-Sosa, S. Tekoglu, S. Stolz, R. Eckstein, C. Teusch, J. Trapp, U. Lemmer, M. Hamburger and N. Mechau, The Compromises of Printing Organic Electronics: A Case Study of Gravure-Printed Light-Emitting Electrochemical Cells, *Adv. Mater.*, 2014, 3235–3240.

51 Q. B. Pei, G. Yu, C. Zhang, Y. Yang and A. J. Heeger, Polymer Light-Emitting Electrochemical-Cells, *Science*, 1995, **269**(5227), 1086–1088.

52 S. Y. Hu and J. Gao, Shaping Electroluminescence with a Large, Printed Bipolar Electrode Array: Solid Polymer Electrochemical Cells with Over a Thousand Light-Emitting p–n Junctions, *ChemElectroChem*, 2020, **7**(7), 1748–1751.

53 S. Tang, A. Sandström, P. Lundberg, T. Lanz, C. Larsen, S. van Reenen, M. Kemerink and L. Edman, Design rules for light-emitting electrochemical cells delivering bright luminance at 27.5 percent external quantum efficiency, *Nat. Commun.*, 2017, **8**(1), 1190.

54 J. Mindemark and L. Edman, Illuminating the electrolyte in light-emitting electrochemical cells, *J. Mater. Chem. C*, 2016, **4**(3), 420–432.

55 E. Zysman-Colman, J. D. Slinker, J. B. Parker, G. G. Malliaras and S. Bernhard, Improved turn-on times of light-emitting electrochemical cells, *Chem. Mater.*, 2008, **20**(2), 388–396.

This journal is © The Royal Society of Chemistry 2023

J. Mater. Chem. C, 2023, **11**, 8263–8273 | **8273**